International Journal of Science and Research (IJSR)
ISSN: 2319-7064
SJIF (2022): 7.942

Study on the Dynamic Sand Carrying Capacity and Large - Scale Physical Simulation Cracking Performance of Medium and Low Viscosity Slick Water

Xiong Ying[1, 2], Chen Nan[1]

[1]Research Institute of Natural Gas Technology, PetroChina Southwest Oil & Gas field Company, Chengdu, Sichuan, China

[2] Shale Gas Evaluation and Exploitation Key Laboratory of Sichuan Province, Chengdu, Sichuan, China

Abstract: ***The dynamic sand carrying capacity and large-scale physical simulation cracking performance of slick water with different viscosities and different types of drag reducing agents were studied, which provided theoretical basis for the optimal design of slick water formulation, In this paper, the dynamic sand carrying capacity and large-scale physical simulation cracking performance of conventional partially hydrolyzed polyacrylamide and hydrophobically associating polymer slick water were studied by using a visual plate dynamic sand carrying capacity test device and a true triaxial large-scale physical model crack initiation test device. The test results showed that the sand equilibrium bank height and slope angle formed by the medium viscosity slick water were relatively small, but the time to reach equilibrium was relatively longer; the sand equilibrium bank height and slope angle formed by the hydrophobic association polymer slick water were both larger than by conventional partially hydrolyzed polyacrylamide slick water at the same viscosity; the fractures formed by hydrophobically associating polymers slick water turned during the extension process, which is more conducive to the generation of branch fractures and unevenly distributed natural fractures in the core with the low viscosity; the extension speed of the fracture formed by the conventional partially hydrolyzed polyacrylamide slick water with the medium viscosity was slow, but the fractures were asymmetrical and had a certain angle of turning. In contrast, the fractures formed by the hydrophobic associating polymer slick water were relatively simple; increasing the displacement was helpful to create a complex fracture network at the same viscosity, and the fracture propagation pattern was determined by the displacement and the stress difference between fractures. These results can provide theoretical support for the on-site selection of slick water viscosity and drag reducing agent type.***

Keywords: Slick Water, Sand Carrying, Cracking, Shale Gas, Triaxial Stress, Viscosity

1. Introduction

Shale gas development mainly relies on large-scale hydraulic fracturing to realize complex fracture network. As one of the key technologies of hydraulic fracturing, slick water has always been a research hotspot. At present, there are many manufacturers of slick water, but with certain differences in products - mainly the viscosity of slick water and the type of drag reducing agents. The viscosity of low viscosity slick water is usually only 1.5-3.0 mPa·s, and medium viscosity slick water is usually 9-12 mPa·s; the types of drag reducing agents mainly include conventional partially hydrolyzed polyacrylamides and hydrophobic associations with certain hydrophobic groups. With the large-scale application of "close segmentation + high strength sand fracturing technology" in shale gas fields, slick water with adjustable viscosity is gradually widely used. Some wells even increased the viscosity to 50-100 mPa·s in the stage of high-intensity sand adding to improve the sand carrying capacity of slick water. Low viscosity slick water features low cost, low friction, poor sand carrying capacity and complex fracture network formed by fracturing. Medium viscosity slick water needs a large amount of drag reducing agents, leading to a high cost and an upward trend in friction with increasing viscosity. But it has strong sand carrying ability and relatively simple fracture network formed by fracturing. Some scholars have successively studied the sand carrying capacity and cracking law of slick water and made certain progress. The sand carrying capacity mainly uses the flat fracture system to simulate the settlement and transport of the proppant in the fractures. The balance height, slope angles and the length of the sand bank are often taken into account when studying the sand carrying capacity of different slick waters. Generally, the balance height of the sand bank increases gradually with time, at gradually slowing rates, and the sand bank in the front half of the fracture is the highest and has the most proppants. Compared with low viscosity slick water, the sand bank formed by linear glue is gentler and delivers better sand carrying capacity. And the dynamic settlement speed is several times that of the static settlement [1-6]. The cracking law mainly uses a fracturing device under triaxial stress to simulate the fracture of rock by different liquids. The process can be divided into four stages: continuous pressurization, well wall cracking, fracture propagation, and fracture penetration. The lower the liquid viscosity, the larger the injection volume, and the more complex the fracture network formed. Besides, the fracture reservoir is prone to form spatial non-planar fracture network[7-12]. Existing studies have neither combined sand carrying capacity and large-scale physical simulation cracking performance of slick water with different viscosities for comprehensive evaluation, nor delved into the influence of different types of drag reducers on the sand-carrying and cracking law. This paper studies the dynamic sand carrying capacity and large-scale physical

simulation cracking performance of different types of drag reducing agents and different viscosities of slick water, with a view to provide theoretical support for the selection and optimization of slick water on site.

2. Experimental Instruments, Methods and Liquids

2.1 Testing Device and Method for Dynamic Sand Carrying Performance of Visual Plate

The device is composed of a liquid tank, a sand tank, a flow meter, a visual plate crack, filtration, and various valves and pipelines. It can be used to observe the sand carrying capacity of slick water in real time and test the sand-laying state. The schematic diagram of the device is shown in Fig. 1.

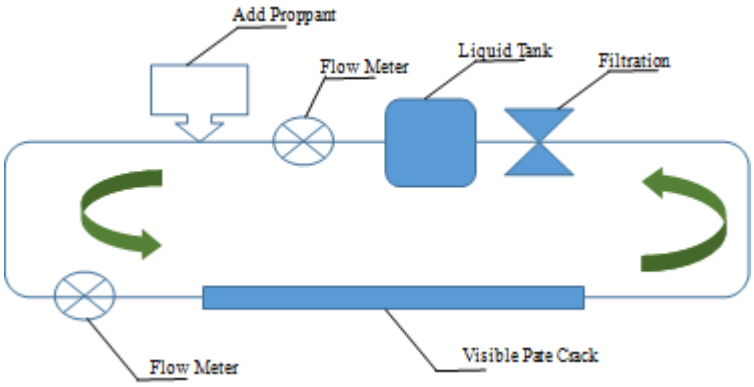

Figure 1: Flow Chart of the Dynamic Sand Carrying Capacity Test Device

Pump slick water into the liquid tank and turn on the device to prepare it for a circulation; open the sand tank, carry the sand into the plate fracture by the liquid while controling the sand ratio, record the flow rate and the time when the sand bank reaches the equilibrium height, and observe the shape of the sand bank. Two parallel steel plates are used to simulate the plate crevice, and a visible observation window is set at the front and rear ends respectively to record the sand dike state by taking photos.

2.2 True Triaxial Large Simulation Cracking Experimental Device and Method

It is composed of a large-size true triaxial test platform, a high-pressure pump injection system, a test metering system, etc.. The device can be stressed to the cube simulated core from three directions: x, y, and z. A 300×300×300 mm cube core was processed from the southern Sichuan shale outcrop, and a circular hole with a diameter of ϕ20 mm and a depth of 20 cm was drilled on the core to simulate the wellbore. The wellbore measures a length of 12 cm and the open hole section 8cm. Spiral steel pipes with diameters of ϕ16 mm and ϕ10 mm were used to make a simulated wellbore with a length of 20 cm and a wall thickness of 3mm. The processed rock sample section is shown in Fig. 2.

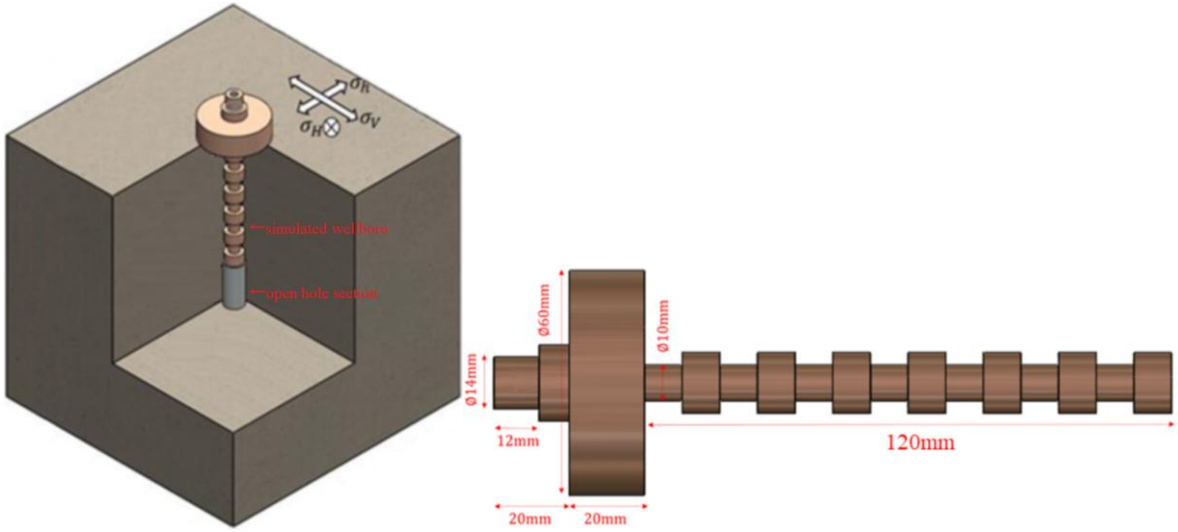

Figure 2: Section of the Processed Rock Sample

By injecting slick water to simulate hydraulic fracturing, the fracture morphology after fracture initiation was studied. The triaxial stress refers to the stress of the reservoir where the outcrop was located. The horizontal principal stress was set to a minimum of 12 MPa and a maximum of 27 MPa, and the vertical principal stress to 20 MPa. The prefabricated fracture was in the same direction as the maximum principal stress. Taking into account the shale bedding and the development of natural fractures, the internal fracture morphology after cracking is more complicated, making direct observation with the naked eye more difficult. Therefore, it is necessary to add a green tracer to the test liquid.

2.3 Experimental Liquid

The experimental liquid used the two drag reducing agents of conventional partially hydrolyzed polyacrylamide and hydrophobic associative polymer to prepare slick water with different viscosities.

Table 1: Basic Parameters of Experimental Liquid

Type of Liquid	Type of Drag Reducing Agent	Viscosity, mPa·s
Low Viscosity Slick Water 1#	Hydrophobically Associating Polymer	1.50
Medium Viscosity Slick Water 1#	Hydrophobically Associating polymer	10.5
Low Viscosity Slick Water 2#	Conventional Partially Hydrolyzed Polyacrylamide	1.50
Medium Viscosity Slick Water 2#	Conventional Partially Hydrolyzed Polyacrylamide	10.5

3. Dynamic Sand Carrying Capacity of Medium and Low Viscosity Slick Water in Visual Plate

When evaluating the dynamic sand carrying capacity in the visual plate, the sand ratio was set to 8%, sand bulk density to 1450 kg/m³, bulk porosity to 30%, and displacement to 0.08m³/min. With reference to the Reynolds number similarity criterion, the corresponding actual displacement on site was 9.7m³/min. The experimental results are shown in Fig. 3 and Table 2.

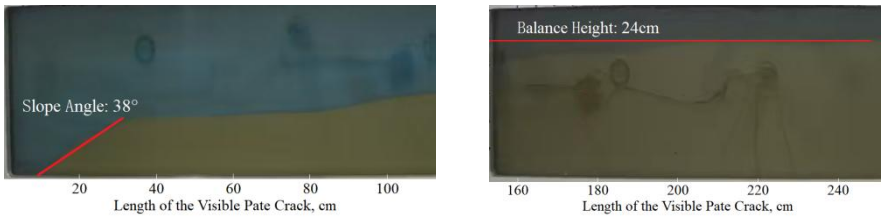

Low Viscosity Slick Water 1# (Left: Front View Window; Right: Rear View Window)

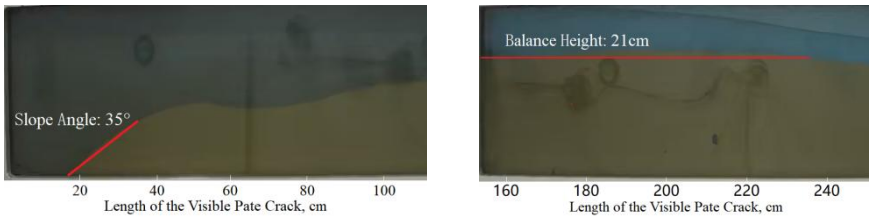

Medium Viscosity Slick Water 1# (Left: Front View Window; Right: Rear View Window)

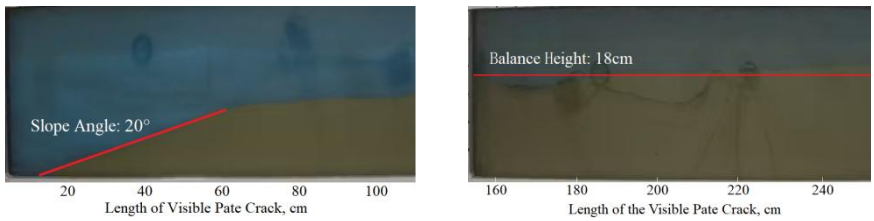

Low Viscosity Slick Water 2# (Left: Front View Window; Right: Rear View Window)

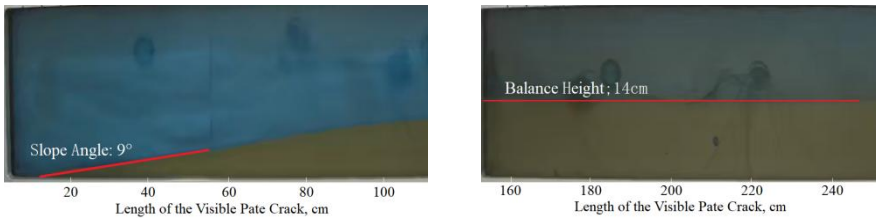

Medium Viscosity Slick Water 2# (Left: Front View Window; Right: Rear View Window)

Figure 3: The Dynamic Sand Carrying Photos of Slick Water with Different Viscosities

Table 2: Parameters of Sand Bank Morphology Analysis

Sand Carrying Liquid	Viscosity of Sand Carrying Liquid, mPa · s	Balance Height, cm	Slope Angle, °	Balance Time, min
Low Viscosity Slick Water 1#	1.50	24	38	6.04
Medium Viscosity Slick Water 1#	10.5	21	35	9.30
Low Viscosity Slick Water 2#	1.50	18	20	4.38
Medium Viscosity Slick Water 2#	10.5	14	9	7.20

It can be seen from Fig. 3 and Table 2 that when slick water with same type carried sand, the balance height and slope angle of the sand bank formed by the medium viscosity slick water were smaller, and the time to reach equilibrium was longer. Slick water depends on viscosity to carry sand. At the high viscosity, the sand bank had stronger ability to move forward. The overall sand bank slope was relatively gentle - without steep slopes when reaching the equilibrium height, and the sand carrying capacity was obviously increased than that in low viscosity. The equilibrium height and slope angle of the sand bank formed by using the drag reducing agent of hydrophobically associating polymer were larger than those by using conventional partially hydrolyzed polyacrylamide. This perhaps caused by the fact that hydrophobically associating polymers had better elasticity than conventional partially hydrolyzed polyacrylamide and could rely on elasticity to improve the sand carrying capacity of slick water.

4. True Triaxial Cracking Law Simulation of Medium and Low Viscosity Slick Water

4.1 Conventional Partially Hydrolyzed Polyacrylamide Slick Water Cracking Simulation

(1) Low Viscosity Slick Water 1#

Fig. 4 shows the cracking and crushing effects of core A. Here, 1.5 mPa • s low viscosity slick water 1# with a displacement of 20 mL/min after continuous injection was used. Fig. 5 is the resulting pump pressure relationship curve. Because core A had some natural fractures and certain porosity and permeability, and the viscosity of slick water 1# was low, so there was a certain amount of filtration in the pump process.

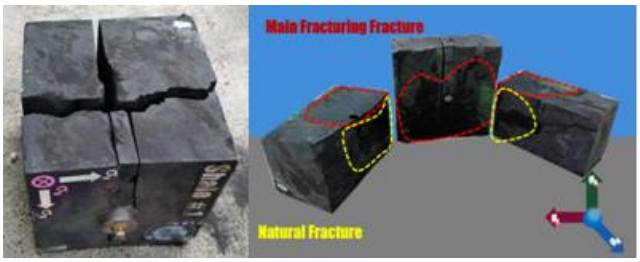

Figure 4: Cracking and Crushing Effects of Core A

Fig. 4 shows that when the pressure reached the fracture pressure, the hydraulic fracture was vertical and extended along the maximum horizontal principal stress to the core boundary; and there were two macroscopic natural fractures at the wellbore axis, the natural crack was opened and extended to the boundary of the sample under the action of slick water. The crack shape was relatively simple, showing a typical cross crack.

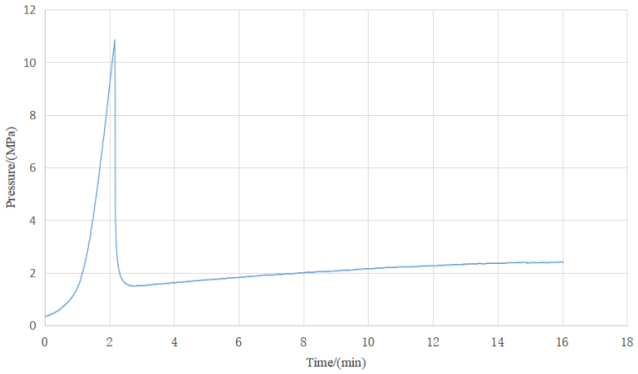

Figure 5: Pump pressure Relationship Curve of Core A

It can be seen from Fig. 5 that during the initial pumping process, the pressure rose and dropped sharply after hitting 11 MPa. This indicates that the hydraulic fracture started to crack at this point, and its fracture pressure was 11 MPa. After cracking, as the slick water continued to filter out to the fracture surface, the fracture extended forward until the core was completely cracked and the pump pressure was reduced to a lower level, and only one hydraulic fracture was formed without other complex fractures. This conclusion was not consistent with the concept of complex fracture formed by low viscosity slick water.

Considering that displacement is also a main factor that affects the complexity of the fracture, the displacement was increased to further test the cracking of the core using the low viscosity slick water 1#. Fig. 6 shows the cracking and crushing effects of core B after continuous injection,. The 1.5 mPa • s low viscosity slick water 1# with a displacement of 40 mL/min was used. Fig. 7 is the resulting pump pressure relationship curve.

Figure 6: Cracking and Crushing Effects of Core B

Fig. 6 shows that there were many fractures and even irregular ones formed after the core was broken. The result suggests that increasing the pumping capacity is helpful to

the formation of complex fracture network at the same viscosity.

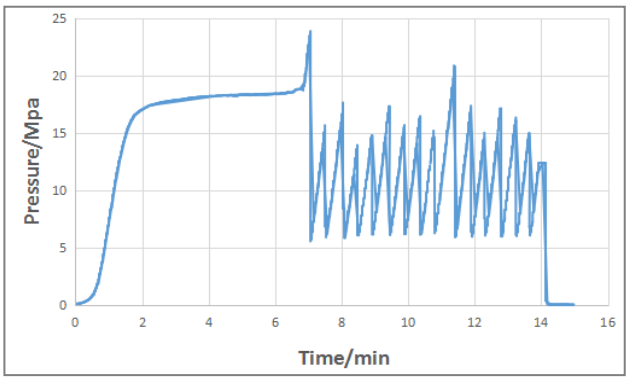

Figure 7: Pump Pressure Relationship Curve of Core B

It can be seen from Fig. 7 that the pump pressure peaked at the 7th minute, with a fracture pressure of about 24 MPa. Then the shock changed, indicating that the fracturing caused multiple hydraulic fractures. Such a result was consistent with the cracking and crushing effects of core B.

(2) Medium viscosity slick water 1#

Fig. 8 shows the cracking and crushing effects of core C after continuous injection. The 10.5 mPa • s medium viscosity slick water 1# with a displacement of 20 mL/min was used. Fig. 9 is the resulting pump pressure relationship curve.

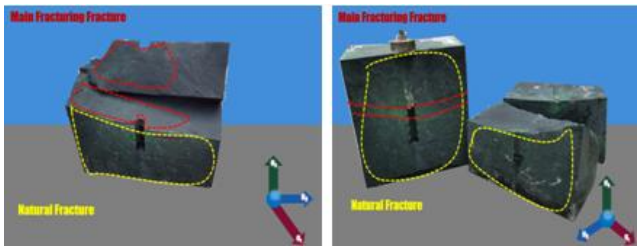

Figure 8: Cracking and Crushing Effects of Core C

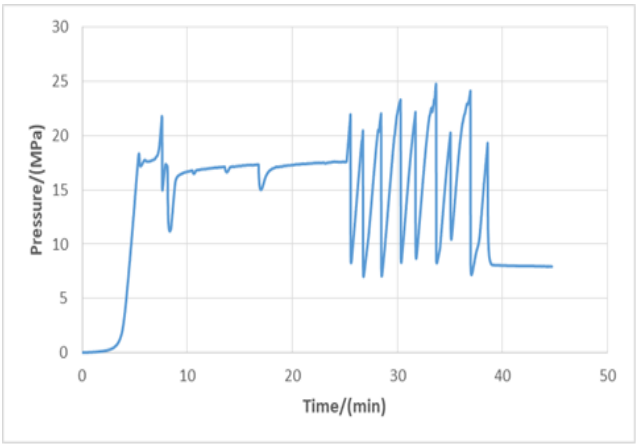

Figure 9: Pump Pressure Relationship Curve of Core C

It can be seen from Fig. 8 and Fig. 9 that when the initial pumping pressure rose rapidly to 18.35 MPa, the core C cracked slightly. The slow extension of the fracture indicated that the distribution range was only near the well zone. Meanwhile, the fracture surface was not completely symmetrical to the wellbore. Because one wing of the fracture expanded in the horizontal bedding direction, while the other turned at a small angle, and extended diagonally upward at an angle of about 30° in the horizontal bedding direction. Therefore, the initial extension speed along the horizontal plane was faster than the extension speed of the other wing. This explained why the crack surface with fast extension was flatter than the one with slow extension.

4.2 Cracking Simulation of Hydrophobic Associating Polymer Slick Water

(1) Low Viscosity Slick Water 2#

Fig. 10 is the cracking and crushing effects of core D after continuous injection, which used 1.5 mPa • s low viscosity slick water 2# with a displacement of 20 mL/min. Fig. 11 is the pump pressure relationship curve at this condition. As the natural fractures of the core were distributed in the periphery of the core, there was fluid loss during the fracturing process.

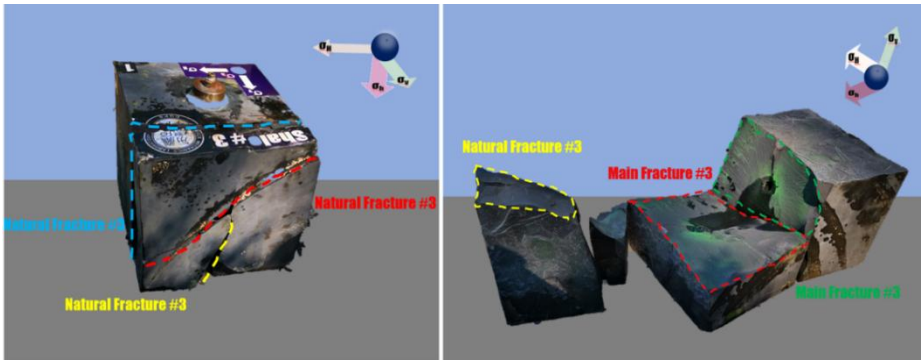

Figure 10: Cracking and Crushing Effects of Core D

It can be seen from Fig. 10 that the large natural fracture, caused by hydraulic pressure, was parallel to the axis of the wellbore. A transverse hydraulic crack was opened at the bottom of the open hole section. It extended in the direction of the maximum horizontal principal stress, communicated with the natural crack after a certain distance, and then extended to the boundary of the core. The surface of the natural fracture was relatively flat with less unevenness, while the hydraulic fractures showed a certain arc and a smooth surface after communicating with natural fractures.

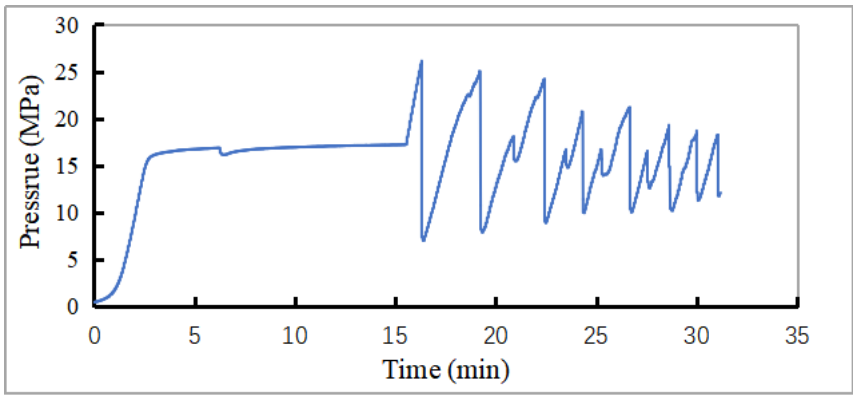

Figure 11: Pump Pressure Relationship Curve of Core D

It can be seen from Fig. 11 that the fracture pressure of core D was 26.1 MPa. After cracking, the pump pressure curve fluctuated frequently, with the amplitude decreasing with time. The hydraulic fracture extended forward continuously, including fracture turning and branch fracture in the far well zone. The time difference between the first two peaks was greater than that of the latter, and the pressure differences between the first few peaks and troughs were very large. Especially, the pressure of the first period rose and dropped rapidly, indicating that the cracking began to extend in the near-well zone.

By comparing and analyzing the cracking performance of low viscosity slick water 1# and 2#, it was found that during the formation of hydraulic fracture in fractured core at 1.5 mPa • s, the fracture turned with the extension of fracture. This demonstrated that at this viscosity, the hydrophobically associating polymer type slick water played a bigger part in the formation of branch fracture and the connection of the unevenly distributed natural fractures in the core.

(2) MediumViscosity Slick Water 2#

Fig. 12 is the cracking and crushing effects of core E after continuous injection, which used 10.5 mPa • s medium viscosity slick water 2# with a displacement of 20 mL/min. Fig. 13 is the resulting pump pressure relationship curve.

Figure 12: Cracking and Crushing Effects of Core E

It can be seen from Fig. 12 that the fracture appeared as a single fracture, which started from only one slit. The fracture was regular and extended along the direction of the maximum stress. Its surface was perpendicular to the direction of the minimum horizontal principal stress. There was fracturing fluid in several other slits, but the hydraulic fracture was not pressed out, indicating that other slits were not pressed open.

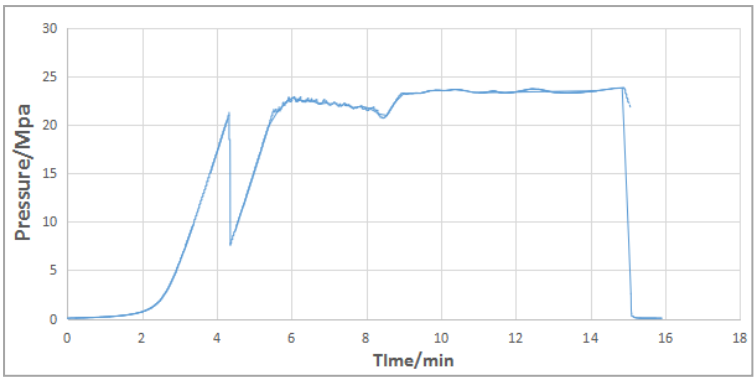

Figure 13: Pump Pressure Relationship Curve of Core E

It can be seen from Fig. 13 that the pressure of core E decayed sharply after hitting the fracture pressure of 20 MPa. Then it continued to rise until leveled at about 23 MPa, indicating that the hydraulic fracture continued to extend at this pressure until the fracture surface broke through the core boundary. This also confirmed the fracture propagation pattern.

By comparing and analyzing the cracking performance of medium viscosity slick water 1# and 2#, it was found that, at 10.5 mPa • s, the fractures extended slowly when conventional partially hydrolyzed polyacrylamide slick water formed hydraulic fractures in fracturing cores, but the fracture surface were asymmetric to the wellbore, and the fractures had a certain turn direction. In addition, the cracks formed by the slick water of hydrophobic associating

polymers were simpler at this viscosity.

5. Conclusions

1) The equilibrium height and slope angle of the sand bank formed by using the drag reducing agent of hydrophobically associating polymer were larger than those by using conventional partially hydrolyzed polyacrylamide. The hydrophobically associating polymers had better elasticity than conventional partially hydrolyzed polyacrylamide and could rely on elasticity to improve the sand carrying capacity of slick water.
2) The balance height and slope angle of the sand bank formed by the hydrophobic association polymer slick water with the low viscosity are both larger than conventional partially hydrolyzed polyacrylamide slick water with the low viscosity. However, the equilibrium heights and slope angles of sand banks formed by the two types of slick water with the medium viscosity are basically the same.
3) At the low viscosity, hydrophobically associating polymer type slick water will change direction with the extension of fracture during the formation of hydraulic fracture in fractured core. The results show that at this viscosity, the hydrophobically associating polymer type slick water delivers better performance in the formation of branch fractures and connection of the unevenly distributed natural fractures in the rock core.
4) At the medium viscosity, when conventional partially hydrolyzed polyacrylamide slick water forms hydraulic fractures in the fractured core, the fracture extension is slow, but the fracture surface is asymmetric, and the fracture has a certain angle of turning. In addition, the fracture formed by hydrophobically associating polymer slick water is more simple.
5) At the same viscosity, increasing the displacement is helpful to create complex fracture networks, and the fracture propagation pattern is determined by the displacement and the stress difference between fractures.

Acknowledgements
Science and Technology Project of PetroChina: Research and application of volume fracturing technology of shale gas in Southwest China (Fund No.: 2021CGCGZ005).

References

[1] Wen Qingzhi, Zhai Hengli, Luo Mingliang, et al. Experimental Study on the Settlement and Migration Law of Fracturing Proppant in Shale Gas Reservoir[J]. Petroleum Geology and Recovery Efficiency. 2012, 19(6):104-107. DOI:10.13673/j.cnki.cn37-1359/te.2012.06.025
[2] Hu Feifei. Yan Chang shale gas reservoir slick-water fracturing fluid and its proppant carrying capacity[D]. Master Thesis of Xi'an Petroleum University, 2014.
[3] Tanhee Galindo. Sand Transport, Does Viscosity Matter?[C]. SPE Liquids-Rich Basins Conference - North America, 7-8 November, Odessa, Texas, USA, SPE-197088-MS, 2019. DOI: https://doi.org/10.2118/197088-MS
[4] Tanhee Galindo. Does Higher Viscosity Improve Proppant Transport? [C]. SPE Oklahoma City Oil and Gas Symposium, 9-10 April, Oklahoma City, Oklahoma, USA, SPE-195192-MS, 2019. DOI: https://doi.org/10.2118/195192-MS
[5] Y. Thomas Hu, Chris Popeney, Pious Kurian. Quantification of Dynamic Sand Settling Velocity in High-Viscosity Friction Reducers and Correlation with Rheology[C]. SPE/AAPG/SEG Unconventional Resources Technology Conference, 22-24 July, Denver, Colorado, USA, URTEC-2019-588-MS, 2019. DOI: https://doi.org/10.15530/urtec-2019-588
[6] Jian Huang, Oswaldo Perez, Tianping Huang, et al. Using Engineered Low Viscosity Fluid in Hydraulic Fracturing to Enhance Proppant Placement[C]. SPE International Hydraulic Fracturing Technology Conference and Exhibition, 16-18 October, Muscat, Oman, SPE-191395-18IHFT-MS, 2018. DOI: https://doi.org/10.2118/191395-18IHFT-MS
[7] Liu Qi. Experimental Study on Fracture Initiation Mode and Propagation Law of Natural Shale During Hydraulic Fracturing[D]. Master Thesis of Liaoning Technical University, 2019.
[8] ZENG Yijin, Zhou Jun, Wang Haitao, et al. Research on true triaxial hydraulic fracturing in deep shale with varying pumping rates[J]. Chinese Journal of Rock Mechanics and Engineering, 2019, 38(9): 1758-1765.
[9] Hou Bing, Cheng Wang, Chen Mian, et al. Experiments on the non-planar extension of hydraulic fractures in fractured shale gas reservoirs[J]. Natural Gas Industry, 2014, 34(12): 81-86. DOI:10.13722/j.cnki.jrme.2018.1542
[10] Hou Bing, Chen Mian, Zhang Baowei, et al. Propagation of multiple hydraulic fractures in fractured shale reservoir[J]. Chinese Journal of Geotechnical Engineering, 2015, 37(6):1041-1045. DOI:10.11779/CJGE201506010
[11] Lou Ye, Zhang Guangqing. Experimental analysis of fracturing fluid viscosity on cyclic hydraulic fracturing[J]. Rock and Soil Mechanics, 2019, 40(S1): 109-117. DOI:10.16285/j.rsm.2018.2256
[12] Olga Kresse, Xiaowei Weng, Dimitry Chuprakov, et al. Effect of Flow Rate and Viscosity on Complex Fracture Development in UFM Model[C]. ISRM International Conference for Effective and Sustainable Hydraulic Fracturing, 20-22 May, Brisbane, Australia, ISRM-ICHF-2013-027, 2013.

Author Profile

Xiong Ying (1981), male, senior engineer, graduated from Southwest Petroleum University with a Ph.D. degree in Applied Chemistry in 2009. At present, have been engaged in the research of chemical technology for oil and gas field development in research institute of natural gas technology, PetroChina southwest oil & gas field company, Tel: +86-028-85604508, email: xiong_y@petrochina.com.cn